Applied Catalysis B: Environmental 202 (2017) 438–445

Contents lists available at ScienceDirect

Applied Catalysis B: Environmental

journal homepage: www.elsevier.com/locate/apcatb

FeOx magnetization enhancing *E. coli* inactivation by orders of magnitude on Ag-TiO_2 nanotubes under sunlight

Marco Mangayayam[a], John Kiwi[a], Stefanos Giannakis[a], Cesar Pulgarin[a,*], Ivica Zivkovic[b], Arnaud Magrez[c], Sami Rtimi[a,*]

[a] Groupe des Procédés Avancés d'Oxydation (GPAO), Ecole Polytechnique Fédérale de Lausanne (EPFL), Station 6, CH-1015, Lausanne, Switzerland
[b] Laboratory of Quantum Magnetism, EPFL-SB-IPHYS-LQMPH, Station 3, CH-1015 Lausanne, Switzerland
[c] EPFL-SB-IPHYS-GCMP, Station 3, CH-1015, Lausanne, Switzerland

ARTICLE INFO

Article history:
Received 23 July 2016
Received in revised form
24 September 2016
Accepted 26 September 2016
Available online 28 September 2016

Keywords:
Ag-TiO_2-FeOx synthesis
E. coli inactivation kinetics
Mechanism
XRD
Radical-scavenging

ABSTRACT

Drastic bacterial enhancement was observed when the Ag(3%)-TiO_2 nanotubes were modified with FeOx (3%) magnetic oxide. On bare TiO_2- nanotubes a reduction of 0.2$\log_{10}$CFU was observed within one hour under simulated low intensity solar light. Under similar conditions, a bacterial reduction of 2.5$\log_{10}$CFU was observed on Ag(3%)TiO_2 increasing to 6.0$\log_{10}$CFU on Ag(3%)-TiO_2-FeOx(3%) magnetic nanotubes. The bacterial inactivation kinetics is strongly influenced by the addition of FeOx. The fast inactivation induced by the composite catalyst seems to involve an increase in the interfacial charge transfer (IFCT) compared to a 2-oxide composite photocatalyst. Stable recycling of the photocatalyst was observed leading to bacterial oxidation. The unambiguous identification of the radical intermediates: OH-radicals, O-singlet and the valence holes vb(h+) on the Ag-TiO_2-FeOx interface showed that the valence band holes vb(h+) were the main oxidative intermediates leading to bacterial inactivation. Nanotubes size, crystallinity and bulk composition of magnetite 1% ($\theta = 51.0^\circ$), anatase 5% ($\theta = 8.9^\circ$), goethite 37.3% ($\theta = 9.0^\circ$), silver 1% ($\theta = 2.7^\circ$) was obtained by the Rietveld refinement for the Ag(3%)-TiO_2-FeOx(3%) nanotubes. The redox chemistry during bacterial inactivation was determined by X-ray photoelectron spectroscopy (XPS).

© 2016 Elsevier B.V. All rights reserved.

1. Introduction

TiO_2 has been has been reported to absorb about 4% of the solar irradiation. A considerable effort has been undertaken during the last few decades to enhance their optical absorption into the visible range by doping, decorating the TiO_2 surface with metals, cations, anions, preparing binary-TiO_2 oxides to enhance the electron-hole separation/reaction kinetics [1–4]. An emerging field of interest is the synthesis of TiO_2 nanotubes and the coupling these nanotubes with cations, metal-oxides and additional composites leading to a higher nanotube sensitization in the visible range [5–7]. TiO_2 nanotubes (TNT) synthesis, dynamics and properties have been addressed due to their potential as photocatalysts [6–8] and incipient use in diverse type of photocells [9,10].

Antibacterial nanostructured titania nanotubes coating incorporated with silver nanoparticles have been reported. They have applications in Ti-implants to avoid post-operation infections [11–13]. The discoloration of the textile dye methyl red under UV-light and the degradation of pollutants by Ag-TiO_2 nanotubes has been recently reported [14,15]. Ag-TiO_2 was observed to accelerate bacterial inactivation when compared with bare TiO_2 under band-gap irradiation [16,17]. To increase the visible absorption of nanotubes, Fe-doping was carried out and their preparation and properties have been reported as well as their use in processes mediating dye degradation [18,19]. Fe-TiO_2 photocatalysts have also been reported recently to be effective in bacterial inactivation under solar irradiation [20,21].

The use of magnetic Ag-TiO_2-Fe_3O_4 composites to degrade chlorophenols has been reported [22]. The degradation of methyl red within 4 h and bacteria within 2 h on Fe-oxide added was reported but adding a much higher amount of Fe compared to the Fe used in the present study [23]. Also Fe_3O_4@TiO_2 core shell nanoparticle epoxide addressing the inactivating *E. coli* under solar light have recently been reported [24]. Iron oxide particles can be manipulated using a magnetic field gradient and have been investigated for their potential use in catalytic degradation of pollutants during water treatment [1,2], in biomedicine and in the biomedical fields [3–5].

* Corresponding authors. Tel.: +41 2169 36150.
E-mail addresses: cesar.pulgarin@epfl.ch (C. Pulgarin), sami.rtimi@epfl.ch (S. Rtimi).

http://dx.doi.org/10.1016/j.apcatb.2016.09.064
0926-3373/© 2016 Elsevier B.V. All rights reserved.

Table 1
Percentage of the Ti, Fe and Ag elements determined by X-ray-fluorescence (XRF) in the Ag-TiO_2 and Ag-TiO_2-FeOx nanotubes prepared in this study.

Sample	Ti	Fe	Ag
3% Ag-TiO_2	85	None	12
1% Ag-TiO_2-FeOx	30.1	68.6	1.2
3% Ag-TiO_2-FeOx	22.7	72.8	3.3
5% Ag-TiO_2-FeOx	20.2	74.2	5.1

We report hereby the synthesis of TiO_2 nanotubes modified by Ag and by magnetic FeOx leading to Ag-TiO_2-FeOx nanotubes. The objective is to show the acceleration of the disinfection kinetics by innovative magnetic nanotubes. This approach avoids the ultrafiltration or centrifugation necessary to separate the spent photocatalyst after the disinfection process. During the synthesis of the Ag-TiO_2-FeOx nanotubes Ag was incorporated into the anatase by exchange followed by calcination. Fe-salts were then deposited on the Ag-TiO_2 nanotubes to add the magnetic properties. This enables the separation of the nanotubes from the solution by magnetic harvesting. A comprehensive, detailed and systematic study is reported in this work on the disinfection kinetics mediated by these novel nanotubes reporting on: the preparation of novel magnetic nanotubes under low intensity sunlight, the semiconductor intervention of the nanotubes in chemical transformations, the mechanism and kinetics of nanotubes during bacterial inactivation and the surface characterization of these innovative nanotubes.

2. Experimental

2.1. Ag-TiO_2-FeOx nanotubes hydrothermal synthesis

The TiO_2 synthesis followed a modified the reported by Kasuga et al., [25] using TiO_2 P25 Degussa Aeroxide (Frankfurt, Germany). Kasuga et al., reported anatase nanotubes with a surface area of 50 m^2/g and presented TEM images of the TiO_2 nanotubes with a diameter of ca. 8 nm and a length ca. 100 nm. To ensure the removal of excess NaCl, the TiO_2 was washed with hot deionized water at 80 °C. Addition of Ag was carried out and the Ag^+ was subsequently reduced with 0.05 M $NaBH_4$ in a cold bath at 5 °C. The change of color from white to yellowish-brown indicates the chemical reduction of Ag. The resulting powders were calcined at 500 °C for 1 h, programming an initial at a heating rate of 250 °C/h. The Fe-incorporation on the Ag-TiO_2 nanotubes was carried out by co-precipitation adding the appropriate amounts of $(NH_4)_2Fe(SO4)_2 \times 6H_2O$ (Sigma Aldrich) and $NH_4Fe(SO_4)_2 \times 12H_2O$ (Sigma Aldrich) in the molar ratio $[Fe^{2+}]$:$[Fe^{3+}]$ of 1:1.5. After drying the powders, the products were harvested using a magnet and washed repeatedly with deionized water and ethanol. The powders were then dried at 70 °C for 3 h.

Table 1 presents the percentage of the Ti, Fe and Ag elements determined by X-ray-fluorescence (XRF) in the Ag-TiO_2 and Ag-TiO_2-FeOx nanotubes prepared in this study. The notation Ag(3%)-TiO_2-FeOx(3%) for the magnetic nanotubes corresponds to the make-up of the solutions used to prepare and load Ag and Fe to the preformed TiO_2 used as the TiO_2 source. The surface percentage of the Ti, Fe and Ag of the nanotubes throughout this study were determined by X-ray-fluorescence (XRF) and are reported in Table 1.

2.2. Evaluation of the E. coli inactivation kinetics during disinfection and irradiation procedures

Samples of *Escherichia coli K12* (*E. coli K12*) were obtained from the Deutsche Sammlung von Mikro-organismen and Zellkulturen GmbH. The Luria-Bertani (LB) broth was prepared in Millipore water and subsequently sterilized [26]. A colony was picked from the pre-cultures and inoculated in 5 mL of LB broth. The vessel was incubated at 37 °C with shaking at a rate of 180 rpm for 8 h. Further dilution was made to a 1% v/v concentration and the solution incubated for 15 h. The *E. coli* were harvested by centrifugation for 15 min at 4 °C. The collected pellets were washed twice and resuspended and sterilized. Aliquots with a bacterial concentration of 10^6 CFU/mL were generally used to follow the disinfection by the magnetic nanotubes irradiating in the cavity of a solar simulator (Atlas GmbH, Hanau, Germany) equipped with a cut-off filter < 310 nm and allow a variation of the light intensity between 25.2 mW/cm^2 and 46.5 mW/cm^2. The spectral emission of the solar simulator is shown in the Supplementary material S1. The samples to evaluate the bacteria CFU/ml were taken every 20 mins by using one milliliter of the aliquots and transferring them to the appropriate Eppendorf tubes for further centrifugation. The samples were then spread-plated on agar (PCA) added to the sterilized Petri dishes. The plates were then incubated for 24 h at 37 °C and the results reported from triplicate bacterial runs.

2.3. Scavenging of the reactive oxygen species (ROS) and analysis of the leached Fe and Ag-ions

To evaluate the role of different ROS, scavengers were employed to identify ^1O by the azide NaN_3, Ethylenediamine tetra-acetic acid (EDTA-2Na) to identify or vb(h+) and Dimethyl sulfoxide (DMSO) to identify the $OH^{\bullet}$-radical. The quantification of the ROS (mainly $OH^{\bullet}$) was carried out based on the method proposed by Hashimoto et al., [27]. The 99% terephthalic acid from Across Chemical Ltd, and the NaOH 98% were Sigma Aldrich and used as received. The photocatalyst was immersed in a 0.4 mmol L^{-1} solution of terephthalic acid dissolved in a 4 mmol L^{-1} NaOH solution. After irradiation, the solution was transferred to a quartz cell. The fluorescence of the 2-hydroxyterephthalic-acid was quantitatively monitored on a Perkin Elmer LS–50 B spectrometer. The spectra were recorded between 400 and 500 nm (scan rate:100 nm/ min) after excitation at 315 nm.

To determine the amount of the Fe-ions (II) an Fe(III) leached in solution the absorbance of Fe(III) was determined by a Ferrozine solution in acetate buffer solution at 562 nm in a Shimadzu UV-1800 spectrophotometer. Then, hydroxylamine hydrochloride (10% w/w) was added to the solution to reduce Fe^{3+} to Fe^{2+} and again the absorbance was measured again but this time of Fe^{2+} after 20 min at 562 nm. Ag-ions estimations in the ppb range were obtained by a Mohr titration to form AgCl that in the presence of chromate ion formed red-brown Ag_2CrO_4.

2.4. X-Ray fluorescence, X-ray diffraction (XRD), X-ray photoelectron spectroscopy (XPS) and magnetic measurements

The X-ray fluorescence (XRF) of Ti, Fe and Ag was evaluated in an Analytical PW2400 spectrometer. The results are shown below in Table 1. The x-rays emitted by the atoms in the sample are collected by a detector, and processed in the analyzer to generate a spectrum showing the x-rays intensity peaks versus their energy. The peak energy identifies the element and its peak area (or intensity) gives an indication of its amount in the sample. The analyzer then uses this information to calculate the sample's elemental composition.

The evolution of powder crystallinity was investigated using X-ray diffraction (XRD) and recorded on an X'Pert MPD PRO from PANalytical equipped with a secondary graphite (002) monochromator and an X'Celerator detector operated in Bragg-Brentano geometry.

The magnetic measurements were performed with a Quantum Design NPMS-Xl 5T Superconducting Interference Device (SQUID) magnetometer. The magnetic powder samples were mixed with a

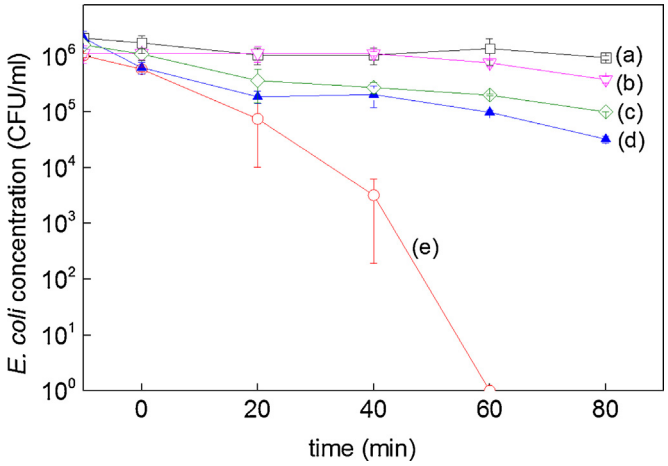

Fig. 1. Bacterial inactivation under low intensity sunlight irradiation (46.5 mW/cm^2) and in the dark mediated by 100 mg nanotube powder in dispersions with different compositions: a) no catalyst control run, b) bare TiO_2 nanotube dispersions under light, c) Ag (3%)-TiO_2 under light, d) Ag(3%)-TiO_2-FeOx(3%) in the dark under and e) Ag(3%)-TiO_2-FeOx(3%) under light irradiation.

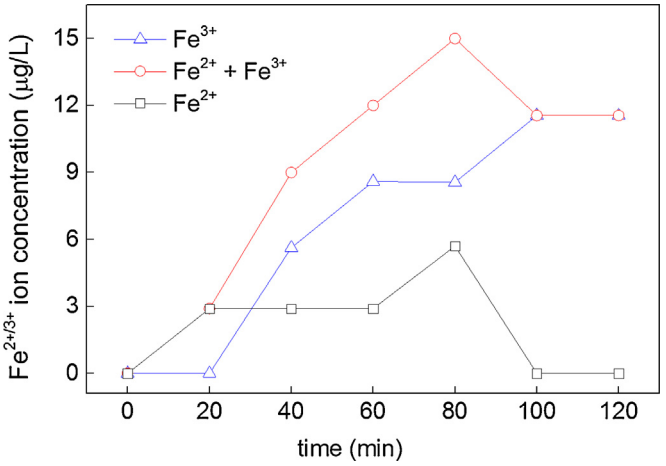

Fig. 2. Determination of the Fe-ions production within the time in the presence of *E. coli* on Ag(3%)-TiO_2-FeOx(3%) nanotubes under solar simulated light (46.5 mW/cm^2).

diluted GE-varnish and then measured at 300 K in a field-sweep sequence 0T → 5T → −5T → 5T.

The X-ray photoelectron spectroscopy (XPS) of the nanotubes was determined using an AXIS NOVA photoelectron spectrometer (Kratos Analytical, Manchester, UK) provided for with monochromatic AlK_a ($h\nu$ = 1486.6 eV) anode. The carbon C1s line with position at 284.6 eV was used as a reference to correct the charging effects. The surface atomic concentration was determined from peak areas using the known sensitivity factors for each element [28,29]. Spectrum background was subtracted according to Shirley [30] and [52,53,60]. The XPS spectral peaks were deconvoluted with a CasaXPS-Vision 2, Kratos Analytical UK.

3. Results and discussion

3.1. *Kinetics of* E. coli *inactivation upon magnetization of the Ag(3%)-TiO_2 nanotubes and catalyst recycling*

Fig. 1 shows the drastic increase in the bacterial degradation kinetics when Ag(3%)-TiO_2-FeOx(3%) nanotubes are irradiated under low intensity sunlight. Within an hour complete bacterial inactivation was attained that is a reduction of 6$\log_{10}$CFU or full bacterial inactivation. During bacterial disinfection, the pH changes from ~6.8 to ~6.1. This pH change is important when discussing the Ag(3%)-TiO_2-FeOx(3%) mechanism leading to bacterial inactivation below in Section 3.4. Ag- and Fe-cations ions intercalate on the TiO_2 lattice of the hydrothermally synthesized nanotubes [31,32] leading a synergistic effect in the Ag(3%)-TiO_2-FeOx(3%) accelerating the bacterial inactivation as shown in Fig. 1, traces e). Fig. 1, shows a very small bacterial reduction of 0.4$\log_{10}$CFU in the absence of nanotubes due to the bacteria absorbing the incoming solar radiation below 340 nm. The Ag(3%)-TiO_2-FeOx(3%) in the dark reduced the bacteria by 1.5$\log_{10}$CFU within 80 min.

Chick-Watson (first order) kinetics (log(C/Co) = k1*t) and Hom's equation (log(C/Co) = −k1*[1-exp(-k2*t)]k3) describe the trend shown for the bacterial inactivation kinetics in Fig. 1. Three different kinetic stages adequately fit the Hom's equation with the parameters: k_1 = bacteria transformation to damaged species, k_2 = damaged bacteria transformation to inactivated species and k_3 = inactivated bacteria transformation to residual products. For the sample Ag(3%)-TiO_2-FeOx(3%), k_1, k_2 and k_3 were 14.5, 0.02 and 4,0 respectively with an R^2 = 0.9741.

Several studies on the activity of Ag-TiO_2 enhancing the photocatalytic transformations of chemicals compared to TiO_2 have been reported [31–36]. Moreover some recent work describes the enhanced microbial inactivation of Ag-TiO_2 composites [37,38]. But the bacterial inactivation of Ag-TiO_2 compared to TiO_2 is strongly dependent on many variables that are difficult to control. During the photocatalysis, the Ag-ions which are the antibacterial agents on the Ag-TiO_2 surface, get reduced on TiO_2 to Ag^0, a non-active antibacterial species [39] due to the cbe- of TiO_2.

Fig. 2 indicates that some Fe(II)(III)-ions were released in the presence of *E. coli*, but the Fe-ions generation was not observed in the absence of bacteria. The kinetics of *E. coli* was also investigated as a function of the amount of Ag in the Ag-TiO_2-FeOx catalyst. Ag(3%) loading led to the fastest inactivation (see Supplementary Fig. S2). A 100 mg powder Ag(3%)-TiO_2-FeOx(3%) catalyst powder led to the fastest bacterial inactivation compared to other amounts of catalysts (see Supplementary Fig. S3).

Under the experimental conditions applied in Fig. 1 an initial load of 10^6 CFU/ml is inactivated within 60 min. But this was not the case for an initial CFU of 10^8/ml load (see Supplementary Fig. S4). This shows the limiting capacity of the active sites on the Ag(3%)-TiO_2-FeOx(3%) to abate bacteria. Fig. 2 shows that the amount of Fe-ions released was far below the cytotoxicity levels for Fe(II)Fe(III) ions [40,41]. The small dissolution of the nanotube surface in the presence of bacteria has been reported due to the presence of Fe^{3+}-siderophores presenting a big affinity for Fe and ability to chelate Fe-ions [42,43]. The oxygenated solution in Fig. 2 shows a much higher level of Fe^{3+}-ions compared to Fe^{2+}-ions since the transformation of $Fe^{2+} \rightarrow Fe^{3+}$ k_1 76 $M^{-1}s^{-1}$ is much higher than the reverse reaction $Fe^{3+} \rightarrow Fe^{2+}$ 2×10^{-2} $M^{-1}s^{-1}$ [1,2,36]. The kinetics of *E. coli* was also investigated as a function of the amount of Ag in the Ag-TiO_2-FeOx catalyst. A catalyst loading of Ag(3%) loading led to the fastest inactivation (see Supplementary Fig. S2).

Fig. 3 shows the recycling of the Ag(3%)-TiO_2-FeOx(3%) nanotube powders up to the 5th cycle. No loss of activity was observed during the repetitive degradation an initial 10^6 CFU bacterial concentration. The Fe leaching from the catalyst surface in the ppb range as shown in Fig. 2, did not affect the bacterial inactivation kinetics up to the 5th cycle as shown in Fig. 3.

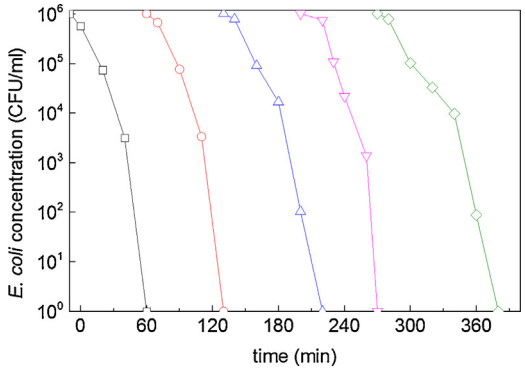

Fig. 3. *E. coli* inactivation e cycles of 3%Ag-TiO_2-FeOx(3%) under low intensity solar simulated light (46.5 mW/cm^2).

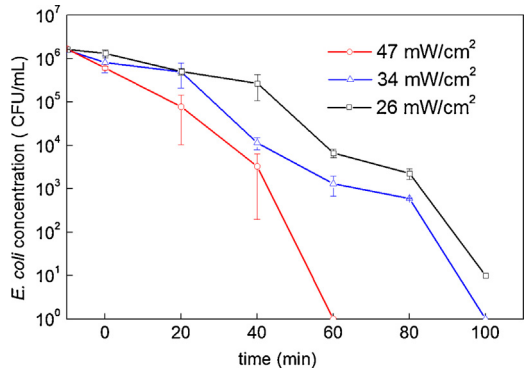

Fig. 5. Dependence of the bacterial inactivation kinetics on the solar simulated solar irradiation dose applied on a sample containing Ag(3%)-TiO_2-FeOx(3%) nanotubes.

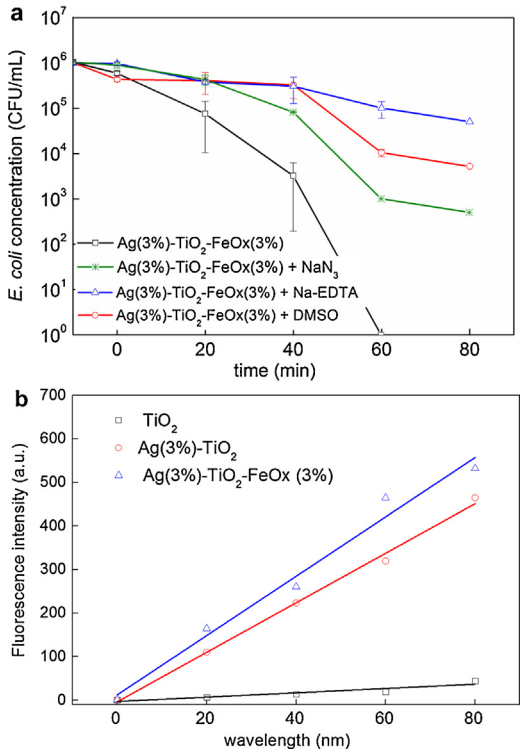

Fig. 4. (a) Baacterial inactivation by Ag(3%)-TiO_2-FeOx(3%) composite nanotubes (100 mg) under solar simulated light (46.5 mW/cm^2): a) no scavengers, b) NaN_3 (0.2 mM) an O-singlet scavenger, c) DMSO (0.2 mM) an OH•-radical scavenger, and d) EDTA-2Na (0.2 mM) a vb(h^+) scavenger. (b) Ebvolution in time of the increase in fluorescence of a solution 2- hydroxyterephthalic acid irradiated up to 80 min. For additional details see Ms text.

3.2. Scavenging of the intermediate oxidative species leading to bacterial inactivation

The contribution of ROS-species and of the valence band holes vb(h^+) during the bacterial inactivation is presented next in Fig. 4a. Fig. 4a presents the scavenging of the radicals during bacterial inactivation under solar light irradiation up to 80 min [1–3,43]. Fig. 4a, trace a) presents the bacterial inactivation, no scavengers added within 60 min, b) trace b) presents the incomplete bacterial inactivation after the addition of 0.2 mM of NaN_3 an O-singlet quencher [44,45]. This compound inactivates bacteria by itself but not at the low concentration of 0.2 mM used during this study [46], c) trace c) shows further inhibition of the bacterial reduction upon addition of 0.2 mM methanol an OH•-radical scavenger and d) trace d) presents the almost initial inhibition of bacterial inactivation upon addition of 0.2 mM EDTA-2Na a well-known vb(h+) scavenger. Benzoquinone a quencher of $O_2^{\bullet -}/HO_2^{\bullet}$ was not assayed since even at very low concentrations it has been reported to inactivate bacteria by itself [1,36,46]. The relative importance of the intermediate radical species leading to bacteria inactivation shown in Fig. 4a is $vbh^+ > OH^{\bullet} >$ O-singlet.

Reactive oxygen species (ROS) are chemically reactive molecules containing oxygen, like superoxide, hydroxyl radical, and singlet oxygen have been widely documented when semiconductor oxides like by TiO_2, Ag_2O and FeOx (mainly Fe_2O_3) undergo band-gap irradiation [1–5,47,48]. Fig. 4b shows the quantitative monitoring for the increase in OH•-radical as a function of the PE-TiO_2 irradiation time. The increase in the fluorescence intensity is proportional to the OH•-radical concentration in solution. Details of the analysis were described in the experimental section [27]. The increase of the fluorescence peaks at 450 nm is shown in Supplementary Fig. S5. The data in Fig. 4b confirms the presence of OH•-radicals during bacterial disinfection as already reported in a qualitatively way in Fig. 4a.

3.3. Ag(3%)-TiO_2-FeOx(3%) nanotubes behaving as semiconductors during to bacterial inactivation

Fig. 5 shows the effect of the applied light dose on the bacterial degradation kinetics. The shorter disinfection kinetics shown in Fig. 5 as a function of a higher light dose providing an increasing amount of photo-generated charges is the evidence for the semiconductor behavior of Ag(3%)-TiO_2-FeOx(3%). In a second step the semiconductor surface charges led to the ROS accounted for in Fig. 4a. No saturation effects for the incoming radiation were observed in the FeOx-TiO_2-PE film since the bacterial inactivation kinetics became shorter as the light intensity was increased.

3.4. Mechanism suggested for the bacterial inactivation on Ag(3%)-TiO_2-FeOx(3%) mediated by a two cascade process

Fig. 6 shows that in the coupled semiconductors the cb(e-) injection and the vb(h+) are a function of their relative potential energy levels. Since the bacterial degradation kinetics was faster on Ag(3%)-TiO_2-FeOx(3%) (Fig. 1, trace e) compared to the one induced by Ag(3%)-TiO_2 (Fig. 1, trace c) this shows that in the presence of FeOx, the additional charge transfer states accelerate the charge transfer from the semiconductors to bacteria.

The mechanism shown in Fig. 6 involves sunlight radiation reaching AgOH. But AgOH decomposes spontaneously to Ag_2O (Eq. (1)) [4–50].

$$AgOH \rightarrow Ag_2O + H_2O(pk = 2.87) \quad (1)$$

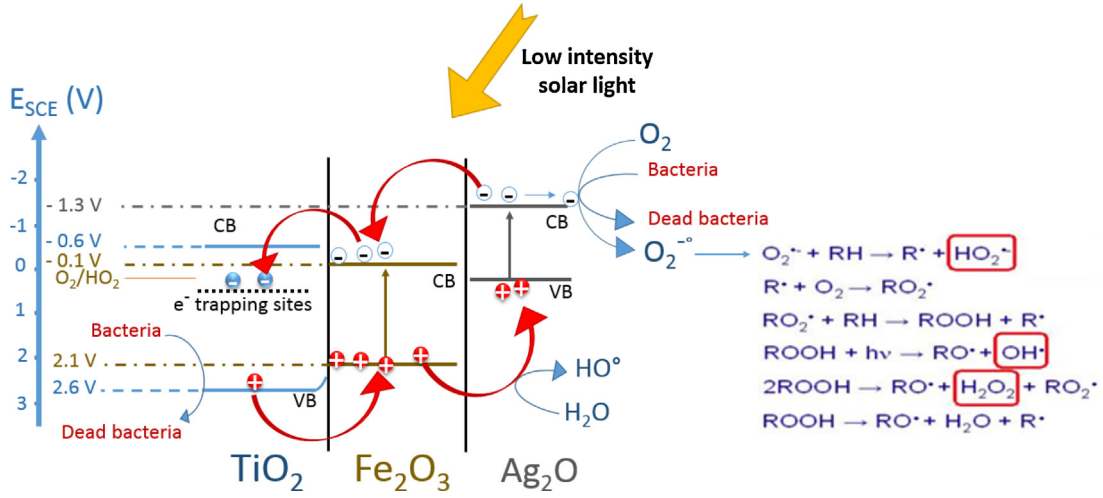

Fig. 6. Ag(3%)-TiO_2-FeOx(3%) interfacial charge transfer as a function of their relative potential energy levels.

This Ag_2O has been reported to be thermodynamically stable region at pH 6–7, the pH domain of bacterial inactivation. Sunlight irradiation photo-activates Ag_2O with a bg ~1.5 eV [43] as noted in Eq. (2):

$$Ag_2O + \text{light} \rightarrow h^+ + e- \quad (2)$$

The transfer of the Ag_2Ocb (e-) to FeOx (mainly goethite FeOOH 37.3%) precludes electron-hole recombination in the Ag_2O and leads to the formation of the highly oxidative radicals inactivating bacteria as shown in the upper right hand side in Fig. 6. Direct and indirect band gaps for nano-goethite with particle sizes as shown in Table 1 have been reported [50]. The Ag_2Ocb (e-) reacts with O_2 (air): $e- + O_2 \rightarrow O_2^{\cdot -}$ giving rise to the radical chain shown in Fig. 6 and concomitantly the Ag_2Ovb(h+) reacts: $h^+ + H_2O \rightarrow OH^\bullet + H^+$. The local pH of the Ag(3%)-TiO_2-FeOx(3%) film was followed during bacterial inactivation and decreased from 6.8 to 6.1. This means that H^+ generation predominates over the generation of OH- displacing the pH in the solution to more acidic values.

The electron transfer from goethite (FeOOH) proceeds to the lower lying anatase electron trapping states located about 0.8–1.0 eV below the TiO_2cb [51] since goethite (cb) is positioned ~0.5-0.8 eV below TiO_2cb [52]. The FeOOH photo-generated charges being very short lived due to its small band gap would increase their lifetime due to cbe- transfer to the anatase (trapping states) or the concomitant vbh+ injection into Ag_2O [48].

In Fig. 6 the goethite-TiO_2 interfacial charge transfer (IFCT) is suggested to involve the following steps:

$$FeOOH + \text{sunligh} \rightarrow FeOOH(e-) + FeOOH(h+) \quad (3)$$

$$FeOOH(e-) + TiO_2 \rightarrow FeOOH + TiO_2(e_{-\text{trapped}-\text{states}}) \quad (4)$$

$$(5)\ FeOOH(e-) + O_2 \rightarrow FeOOH + O_2^- \quad (5)$$

$$O_2^- + H^+ \rightarrow HO_2^\bullet \rightarrow \text{ROS(reactiveoxygenspecies)} \quad (6)$$

$$TiO_2(e_{-\text{trappedsite}}) + O_2 \rightarrow TiO_2 + O_2^- \rightarrow \text{radicals} \quad (7)$$

$$TiO_2(h+) + \text{bacteria} \rightarrow CO_2 + H_2O + \text{residues} \quad (8)$$

An alternative shorthand mechanism is suggested below in the overall Eq. (9).

$$\begin{aligned} &\text{bacteria} + [Ag_2O\text{-}TiO_2\text{-}FeOOH] + \text{sunlight} \\ &\rightarrow [\text{bacteria}\cdots Ag_2O*\text{-}TiO_2\text{-}Fe*OOH] \\ &\rightarrow [\text{bacteria}*\cdots Ag_2O\text{-}TiO_2\text{-}FeOOH] \\ &\rightarrow [\text{bacteria}^+\cdots Ag_2O\text{-}TiO_2(e-)\text{-}FeOOH] \end{aligned} \quad (9)$$

Table 2
Summary of average crystallite size calculated from the strongest peak signal.

Sample no. (% Ag)	2θ (101)	β (FWHM)	D (nm)
Sample 2 (0%)	25.25	0.4856	17.01 nm
Sample 3 (1%)	25.28	0.5103	16.17 nm
Sample 4 (3%)	25.22	0.5825	14.13 nm
Sample 5 (5%)	25.25	0.6729	12.20 nm

3.5. X-Ray diffraction (XRD), particle size, magnetic properties and visual perception of samples

Fig. 7a shows the XRD-spectra for Ag (1%, 3%, 5%)-TiO_2 nanotube powder with the TiO_2 peaks and Ag-peaks. The XRD became broader upon an increasing Ag-concentration as reported by Toledo et al., [53] and Lei et al., [54]. Table 1 summarizes the size of TiO_2 anatase crystallites, calculated from the peak fitting of the (101) reflection in the XRD spectrogram by way of the Debye-Scherrer noted below in Eq. (10).

$$D = \frac{k\lambda}{\beta cos\theta} \quad (10)$$

Where, D = crystallite size (nm), k = shape factor (usually taken as 0.89), λ = X-ray wavelength (taken as 0.15406 nm), β = FWHM (radians), θ = Bragg's diffraction angle (radians).

The presence of Ag^o in the Ag-TiO_2 samples was detected by XRD along additional peaks commonly ascribed to Ag_2O. Table 2 shows that Ag reduces the crystallite size of anatase in agreement with a study recently reported [46]. In this reference, the Ag-TiO_2 was prepared starting from butyl titanate as titanium source, adding the desired amount $AgNO_3$ and after a sol-gel drying the gel at 60 °C, calcining the TiO_2, Ag-TiO_2 at 400 °C and 500 °C. By using Scherrer's equation, the size of TiO_2 samples was found to be 34 nm, decreasing to 12 nm after heating at 400 °C and to 10.9 nm after heating at 500 °C. The drastic reduction of the TiO_2 crystallite size upon addition of Ag was explained to the effect of Ag inhibiting in the TiO_2 gel grain growth. In the present study we have used pre-formed TiO_2 P25 Degussa Aeroxide (Frankfurt, Germany) adding Ag as described in the Experimental section 2.1 and subsequently calcining at 500 °C for 1 h. The reduction in the particle size upon Ag-doping was estimated by the Scherrer's Eq. (10) and the results shown in Table 2. Upon addition of Ag s the sample size shows a reduction of the TiO_2 size from 17 to 12 nm for an Ag(5%) doped sample. The reduction in the crystallite sizes is ascribed to

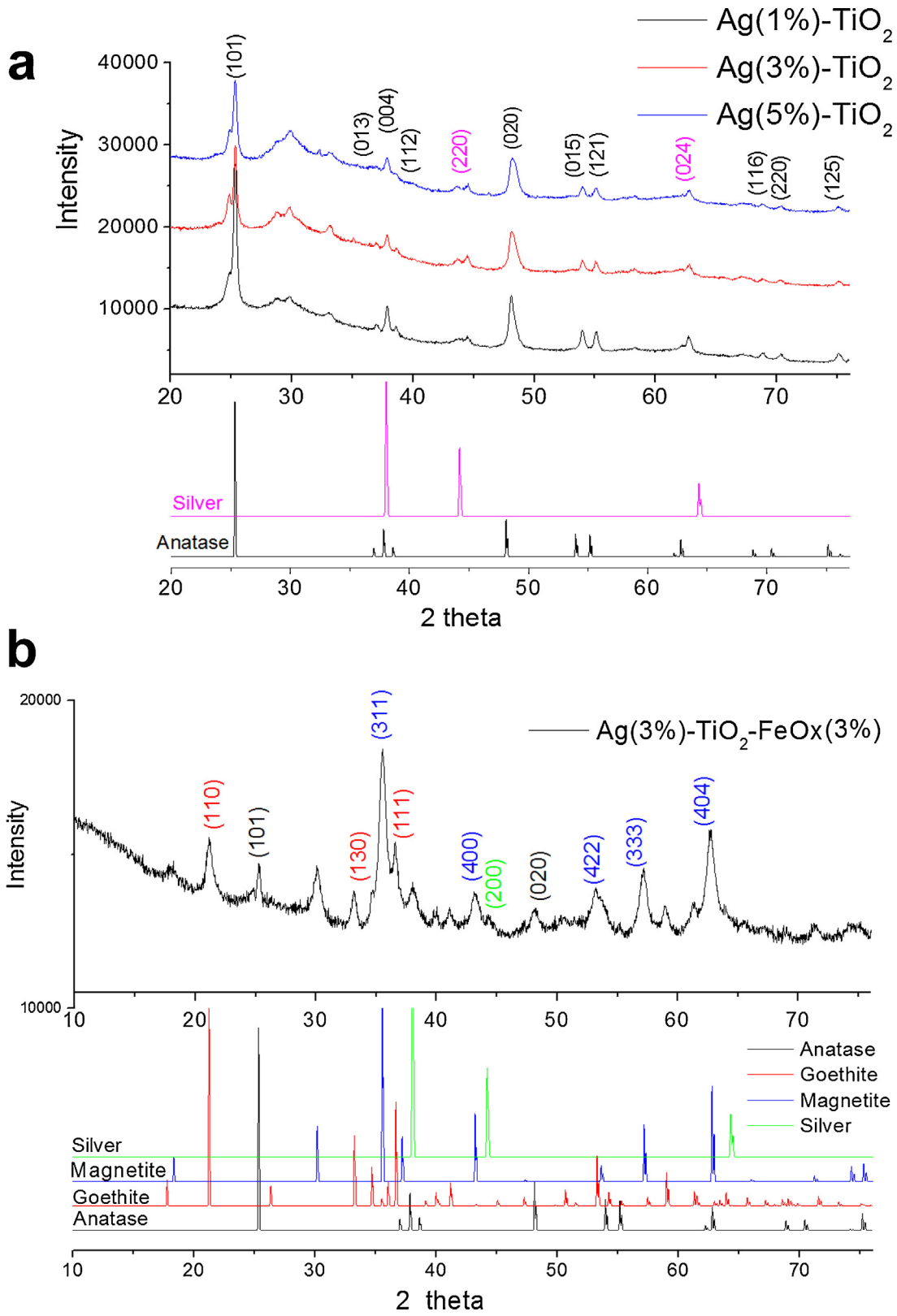

Fig. 7. (a) X-aRay diffraction of 1%, 3% and 5% Ag-TiO_2 prepared for nanotubes referenced to pure Ag and TiO_2 calcined anatase powders. (b) X-bRay diffraction of Ag(3%)-TiO_2-FeOx(3%) nanotubes referenced to anatase, goethite, magnetite and silver powders.

an increase in the TiO_2 crystallite compactness as the amount of Ag in contact with the TiO_2 sample increases. Samples were calcined for the same time (1 h) at 500 °C. In the supplementary Figs. S6, the XRD of TiO_2 P25 Degussa is shown along the XRD of the nanotubes heated at 500 °C. A close resemblance was observed due to the presence of anatase and an additional phase with a monoclinic symmetry. The complete transformation for $H_2Ti_3O_7$ to titanate

at 500 °C was reported by Tsai and Teng reporting atomic plane d-spaces of 0.58 [54].

Upon incorporation of the magnetic component FeO_X, the XRD of the Ag(3%)-TiO_2-FeOx(3%) nanotube changes considerably and this is seen by inspection of Fig. 7b. The composition of this sample as determined by the Rietveld refinement were: magnetite 1% (θ = 51.0°), anatase 5% (θ = 8.9°), goethite 37.3% (θ = 9.0°), silver 1% (θ = 2.7°) and the rest was rutile and a more significant percentage of TiO_2 amorphous. The Rietveld refinement implies material characterization by neutron and X-ray diffraction to obtain the reflections (peaks in intensity) at certain positions [55]. A peak reduction in the anatase reflections of (101) and (020) was observed on the magnetite and goethite peaks. It has been reported by Selmani et al., [56] and Grover et al., [57] that the magnetite/goethite incorporation in a nanocomposite was a function of: the applied temperature, the co-precipitation pH in the aqueous solution and the sample exposition to N_2 or air during heat treatment/calcination. Using eq.(10) in the Ag-TiO_2-FeO_x nanocomposite, the estimated crystallite sizes obtained using the reflections of (311) for magnetite and (110) for goethite were 7.8 nm and 5.1 nm respectively. The magnetization of the samples is shown in Fig. S7 of the Supplementary material. In the supplemental material the samples S7a TiO_2-FeOx(0.5%); S7b Ag(1%)-TiO_2-FeOx(3%); S7c Ag(3%)-TiO_2-FeOx(3%) and S7d Ag(5%)-TiO_2-FeOx(3%) present magnetic properties. The sample S7e TiO_2-FeOx (1%) is paramagnetic showing saturation behavior. The magnetization level detected in the sample S7e was about a hundred times smaller compared to the samples S7b, S7c and S7d.

The isoelectric point (IEP) of goethite has been reported with values 7.5–8.5. At a pH 6–7 used during the bacterial inactivation, the surface Fe-OH_2^+ interacts electrostatically with bacteria [58]. Nano-goethite with a band-gap of 2.2 eV, under sunlight irradiation generates ROS as shown in Fig. 4a. Goethite being a weak magnetic material will decrease the magnetization of magnetite (band gap of 0.1 eV) [57].

The significant difference in the visible perception of TiO_2, Ag-TiO_2 and Ag(3%)-TiO_2-FeOx(3%) nanotube powders is seen in Fig. 9a,b. The dark coloring effect by FeOx is readily seen in Fig. 9b.

3.6. Surface composition and redox shifts detected by XPS during bacterial inactivation

Fig. 8a(a) shows the initial values (time zero) for the binding energies of the Ti- found in the XPS spectrogram of the Ag(3%)-TiO_2-FeOx(3%) nanotubes. The peak positions reported in Fig. 8 were consistent with the values reported in references [28,29]. Fig. 8a(b) shows the corresponding XPS peaks after one bacterial inactivation. A shift of 0.4 eV for TiO_2 and TiOH was observed after bacterial inactivation (Fig. 8a(b)). Shifts ≥0.2 eV imply the appearance in the XPS spectrogram of new species on the catalysts surface [30,58]. The interaction of the bacteria with the photocatalyst surface comprises the electrostatic interaction of the positively charged TiO_2, Fe_2O_3 and Ag_2O oxides with the negative charged *E. coli*.

Fig. 8b(a) and (b) report the shifts of the AgOH peak from 366.8 eV to 366.0 eV. The Ag_2O peak remained stable before and after bacterial inactivation showing only a shift of ~0.1 eV. The small difference in the relaxation energies for Ag(I) and (Ag II) is responsible for their very close BE-energies [59,28] and the assignment of these peaks is complicated by the electrostatic charging for Ag-oxides. Fig. 8c(b) presents XPS-peak shifts after one hour with respect to Fig. 8c(a) at zero time comprising: a) a small shift for FeOOH of 0.2 eV, b) a stronger shift for the magnetic species Fe_3O_4 of 0.3 eV and c) a FeO peak shift of 0.2 eV. The observed XPS-shifts indicate that new species appear in the FeOx nanoparticles after bacterial inactivation.

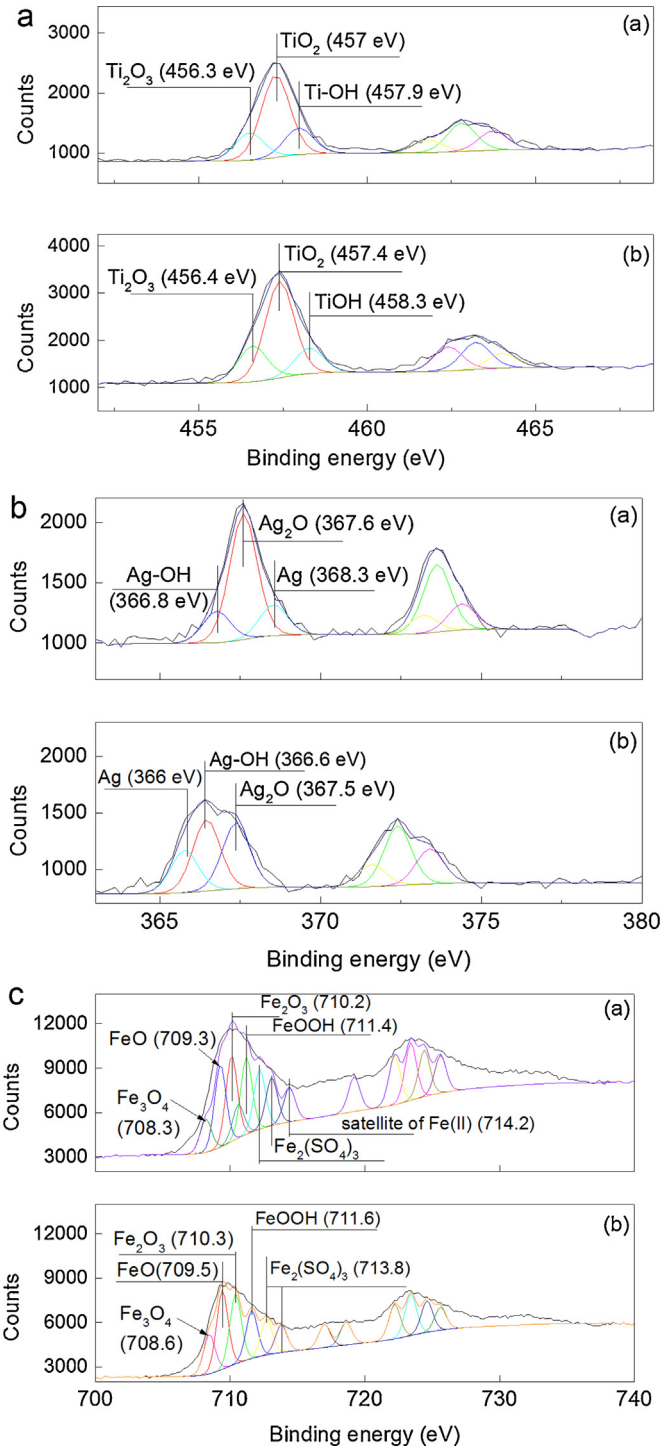

Fig. 8. (a) Tai2p deconvolution of the XPS peaks of Ag(3%)-TiO_2-Fe(3%) nanotubes: (a) before bacterial inactivation and (b) after bacterial inactivation within one hour under low intensity solar light (46.5 mW/cm^2). (b) Abg3d deconvolution of the XPS peaks for Ag(3%)-TiO_2-Fe(3%) nanotubes: (a) before bacterial inactivation and (b) after bacterial inactivation within one hour under low intensity solar simulated light (46.5 mW/cm^2). (c) Fce2p deconvolution in Ag(3%)-TiO_2-Fe(3%) nanotubes: (a) before bacterial inactivation and (b) after bacterial inactivation under low intensity within one hour under solar simulated light (46.5 mW/cm^2).

4. Conclusions

In summary, a synergistic effect between Ag and Fe in Ag(3%)-TiO_2-FeO_x (3%) accelerate the bacterial reduction of *E. coli* under low intensity solar irradiation within 60 min. The kinetics of bac-

Fig. 9. (a) Paowder samples of Ag(1%)-TiO_2, Ag(3%)-TiO_2 and Ag(5%)-TiO_2.

terial inactivation on Ag(3%)-TiO_2-FeOx(3%) nanotubes was seen to proceed with a 3.5$\log_{10}$CFU order of magnitude increase over the bacterial inactivation mediated by Ag(3%)-TiO_2 nanotubes. The effect of the variation of the applied solar dose suggests that the bacterial inactivation kinetics is a function of the photo-generated charges on the oxides making up the photocatalyst. The transients leading to bacterial inactivation such as: h_{vb}^+, HO_2^-, and ^{1}O-singlet were unambiguously identified. The Fe-cation leached in ppb amounts during bacterial inactivation does not to have a significant effect on the bacterial degradation kinetics due to its low concentration. A mechanism of reaction is suggested based on the potential energy position of the electronic bands making up the Ag(3%)-TiO_2-FeOx(3%) nanotubes. The surface properties of the nanotubes were investigated by XRD and XPS. Bacterial inactivation proceeded without adding chemicals on photo-stable and reusable nanotubes. The nanotubes were magnetically recoverable by an external magnet for subsequent reuse.

Acknowledgments

We thank the EPFL and the Swiss National Science Foundation (SNF) project (200021-143283/1) for the financial support. We thank Prof. H. Ronnow for providing the magnetization equipment and measurement.

Appendix A. Supplementary data

Supplementary data associated with this article can be found, in the online version, at http://dx.doi.org/10.1016/j.apcatb.2016.09.064.

References

[1] A. Fujishima, X. Zhang, D. Tryk, Surf. Sci. Rep. 63 (2008) 515–582.
[2] J. Schneider, M. Matsuoka, M. Takeuchi, J. Zhang, Y. Horiuchi, M. Anpo, D. Bahnemann, Chem. Rev. 118 (2014) 9919–9986.
[3] H. Foster, I. Ditta, S. Varghese, A. Steele, Appl. Microbiol. Biotechnol. 90 (2011) 1847–1868.
[4] M. Pelaez, N. Nolan, S.C. Pillai, M. Seery, Po. Falaras, A. Kontos, P.S.M. Dunlop, J. Hamilton, J.-A. Byrne, K. O'Shea, M. Entezari, D. Dionysiou, Appl. Catal. B 125 (2012) 331–345.
[5] J.-A. Byrne, P.S.M. Dunlop, J.H. Hamilton, P. Fernadez-Ibanes, I. Polo-Lopez, P. Kumar Sharma, A.S. Vennard, Molecules 20 (2015) 5574–5615.
[6] D.V. Bavykin, J.M. Friederich, F.C. Walsh, Adv. Mater. 18 (2006), 2807–2024.
[7] D.V. Bavykin, J.M. Friederich, A.A. Lapkin, F.C. Walsh, Chem. Mater. 18 (2006) 1124–1129.
[8] J. Podporska-Carroll, E. Panaitescu, B. Quilty, L. Wang, L. Menon, S.C. Pillai, Appl. Catal. B 176–177 (2015) 70–75.
[9] M. Grandcolas, A. Louvet, N. Keller, N. Keller, K.R. Thampi, Angew. Chem. Int. Ed. 48 (2008) 161–164.
[10] E. Neville, M. Mattle, D. Loughrey, B. Rajesh, M. Rahman, J. Mac Elroy, A. Sullivan, K.R. Thampi, J. Phys. Chem. C 116 (2012), 16511–11652.
[11] K.M. Seery, R. George, P. Floris, S.C. Pillai, J. Photochem, Photobiol. A 189 (2007) 258–263.
[12] H. Zhang, G. Wang, D. Chen, X. Lv, J. Li, Chem. Mater. 20 (2008) 6543–6549.
[13] V. Etacheri, C. Di Valentine, J. Schneider, D. Bahnemann, S. Pillai, J. Photochem. Photobiol. C 25 (2015) 1–29.
[14] F. Petronella, M.L. Curri, M. Striccoli, E. Fanizza, C. Mateo-Mateo, R.A. Alvarez-Puebla, T. Sibillano, C. Giannini, M.A. Correa-Duarte, R. Comparelli, Appl. Catal. B 178 (2015) 91–99.
[15] S. Murgolo, F. Petronella, R. Ciannarella, R. Comparelli, A. Agostiano, M.L.-Curri, G. Marcelo, Catal. Today 240 (2015) 114–124.
[16] A. Cavallaro, S. Taheri, K. Vasilev, Biointerphases 9 (2014) 029005.
[17] K. Vasilev, Z. Poh, K. Kant, J. Chan, A. Michelmore, D. Losic, Biomaterials 31 (2010) 532–540.
[18] L. Deng, S. Wang, D. Liu, B. Zhu, W. Huang, S. Wu, S. Zhang, Catal. Lett. 29 (2009) 513–518.
[19] J. Yu, Q. Xiang, M. Zhou, Appl. Catal. B 90 (2009) 595–602.
[20] J. Zhu, W. Zheng, B. He, J. Zhan, M. Anpo, J. Mol. Catal. A 216 (2004) 35–43.
[21] S. Rtimi, R. Sanjines, J. Kiwi, C. Pulgarin, M. Bensimon, I. Kmehl, V. Nadtochenko, RSC Adv. 5 (2015) 101751–101759 (and references therein).
[22] S. Chang, W. Chung, S. Yu, S. Lee, Desalin. Water Treat. 4 (2015) 3646–3653.
[23] A. Bokare, H. Singh, M. Pai, R. Nair, S. Sabharwal, A. Athawale, Mater. Res. Express 1 (2014) 046111.
[24] T. Nardi, S. Rtimi, C. Pulgarin, Y. Leterrier, RSC Adv. 5 (2015) 105416–105421 (and references therein).
[25] T. Kasuga, M. Hiramatsu, A. Hoson, T. Sekino, K. Niihara, Langmuir 14 (1998) 3160–3163.
[26] S. Giannakis, E. Darakas, A. Escalas-Cañellas, C. Pulgarin, Chem. Eng. J. 281 (2015) 588–598.
[27] K. Ishibashi, A. Fujishima, T. Watanabe, K. Hashimoto, Eectrochem. Commun. 2 (2000) 207–210.
[28] M. Wagner, M. Riggs, E. Davis, G. Müllenberg, Handbook of X-ray Photoelectron Spectroscopy, Perkin-Elmer Corporation, Physical Electronics Division, Minnesota, 1979.
[29] J. Nogier, M. Delamar, P. Ruiz, M. Gratzel, R. Thampi, J. Kiwi, X-Ray photoelectron spectroscopy of TiO_2/V_2O_5, Catal. Today 20 (1994) 109–123.
[30] A.D. Shirley, Corrections of electrostatic charged species in XSP-spectroscopy, Phys. Rev. B 5 (1972) 4709–4716.
[31] J. Yu, J. Xiong, B. Cheng, Sh. Liu, Appl. Catal. B 60 (2005) 221.
[32] X. Wang, R. Yu, K. Wang, G. Yang, H. Yu, Chin. J. Catal. 36 (2015) 2211–2218.
[33] Ch. P. Sajan, S. Wageh, A. Al Ghamdi, J. Yu, Sh Cao, Nano Res. 9 (2016) 3–27.
[34] Tu. Du, D. Tang, G. Zhang, X. Wu, Chin. J. Catal. 36 (2015) 2219–2228.
[35] J. Fu, Sh. Cao, J. Yu, J. Metereomics 1 (2015) 124–133.
[36] L.G. Devi, R. Kavitha, Appl. Surf. Sci. 360 (2016) 601–622.
[37] S. Tallosy, L. Janovak, E. Nagy, A. Deak, A. Juhasz, E. Czapo, N. Buzas, I. Dekany, Appl. Surf. Sci. 371 (2016) 139–150.
[38] A. Zielinska-Jurek, Z. Wei, I. Wysocka, P. Szweda, E. Kowalska, Appl. Surf. Sci. 353 (2015) 317–325.
[39] T. Yuranova, A.G. Rincon, A. Bozzi, S. Parra, C. Pulgarin, P. Albers, J. Kiwi, J. Photochem. Photobiol. A 161 (2003) 27–34.
[40] S. Chernousova, M. Epple, Angew. Chem. Int. Ed. 52 (2013) 1636–1653.
[41] C. Lee, Y. Kim, I. Lee, L. Nelson, J. Yoon, L. Sedlak, Environ. Sci. Technol. 42 (2008) 4927–4933.
[42] S. Chang, H. Lamm, H. Steven, Int. J. Toxicicol. 22 (2003) 175–186.
[43] J.A. Lemire, J.J. Harrison, R.J. Turner, Nat. Rev. Microbiol. 11 (2013) 371–384.
[44] A. Sychev, V. Isak, Russ. Chem. Rev. 64 (1995) 1105–1129.
[45] C. Ruales-Lonfat, N. Benitez, A. Sienkiewicz, C. Pulgarin, Appl. Catal. B 160 (2014) 286–297.
[46] J. Bandara, J. Kiwi, New J. Chem. 23 (1999) 717–724.
[47] S. Chang, H. Lamm, H. Steven, Int. J. Toxicol. 22 (2003) 175–186.
[48] S. Rtimi, R. Sanjines, J. Kiwi, C. Pulgarin, M. Bensimon, I. Khmmel, V. Nadtochenko, RSC Adv. 5 (2015) 101751–101759.
[49] O. Baghriche, S. Rtimi, A. Zertal, C. Pulgarin, R. Sanjines, J. Kiwi, Appl. Catal. B 174 (2015) 376–382 (and references therein).
[50] G. Biedermann, G. Sillèn, Acta Chem. Scand. 14 (1969) 0717.
[51] J. Yu, J. Ran, Energy Environ. Sci. 4 (2011) 1364–1371.
[52] H. Zhang, M. Baynet, S. Fernando, B. Legg, M. Zhu, J. Penn, J. Banfield, J. Phys. Chem. C 115 (2011) 17704–17710.
[53] J. Antonio-Toledo, M. Jacome-Cortes, C. Chavez-Angeles, E. Lopez Salinas-Lopez, P. Quintana, Langmuir 25 (2009) 10195–10201.
[54] C. Tsai, H. Teng, Chem. Mater. 16 (2004) 4352–4358.
[55] H.M. Rietveld, J. Appl. Crystallogr. 22 (1969) 65–71.
[56] A. Selmani, M. Špadina, M. Plodinec, M. Delačn, M.G. Willinger, J. Lützenkirchen, D. Gafney, E. Redel, J. Phys. Chem. C 119 (2015) 19729–19742.
[57] S. Grover, S. Singh, B. Pal, Appl. Surf. Sci. 280 (2013) 366–372.
[58] S. Rtimi, O. Baghriche, C. Pulgarin, R. Sanjines, J. Kiwi, RSC Adv. 2 (2013) 8591–8595.
[59] S.W. Gaarenstrom, N. Winograd, J. Chem. Phys. 67 (1977) 3500–3506.